Model-independent determination of the axial mass parameter in quasielastic neutrino-nucleon scattering

Bhubanjyoti Bhattacharya, Richard J. Hill, and Gil Paz

Model independent determination of the axial mass parameter in quasielastic neutrino-nucleon scattering

BHUBANJYOTI BHATTACHARYA, RICHARD J. HILL AND GIL PAZ

Enrico Fermi Institute and Department of Physics
The University of Chicago, Chicago, Illinois, 60637, USA

Abstract

Quasielastic neutrino-nucleon scattering is a basic signal process for neutrino oscillation studies. At accelerator energies, the corresponding cross section is subject to significant uncertainty due to the poorly constrained axial-vector form factor of the nucleon. A model-independent description of the axial-vector form factor is presented. Data from the MiniBooNE experiment for quasielastic neutrino scattering on ^{12}C are analyzed under the assumption of a definite nuclear model. The value of the axial mass parameter, $m_A = 0.85^{+0.22}_{-0.07} \pm 0.09 \, \text{GeV}$, is found to differ significantly from extractions based on traditional form factor models. Implications for future neutrino scattering and pion electroproduction measurements are discussed.

1 Introduction

High statistics neutrino experiments are probing the hadronic structure of nuclear targets at accelerator energies with ever greater precision. Extracting the underlying weak-interaction parameters, or new physics signals, requires similar precision in the theoretical description of the strong interactions.

A basic cross section describes the charged-current quasielastic scattering process on the neutron,

$$\nu_\mu + n \rightarrow \mu^- + p \,. \tag{1}$$

Recent evidence indicates a tension between measurements of this process in neutrino scattering at low [1, 2, 3, 4] and high [5] neutrino energies, and between results from neutrino scattering and results inferred from pion electroproduction [6]. In particular, with a commonly used dipole ansatz for the axial-vector form factor of the nucleon,

$$F_A^{\text{dipole}}(q^2) = \frac{F_A(0)}{\left[1 - q^2/(m_A^{\text{dipole}})^2\right]^2} \,. \tag{2}$$

different experiments have reported values for the so-called axial mass parameter m_A^{dipole}. World averages reported by Bernard et al. [6] find comparable values obtained from neutrino scattering results prior to 1990, $m_A^{\text{dipole}} = 1.026 \pm 0.021 \, \text{GeV}$, and from pion electroproduction, $m_A^{\text{dipole}} = (1.069 - 0.055) \pm 0.016 \, \text{GeV}$.[1] The NOMAD collaboration reports [5] $m_A^{\text{dipole}} = 1.05 \pm 0.02 \pm 0.06 \, \text{GeV}$. In contrast, MiniBooNE reports [3] $m_A^{\text{dipole}} = 1.35 \pm 0.17$ GeV, and other recent results from the K2K SciFi [1], K2K SciBar [7] and MINOS [8] collaborations similarly find central values higher than the above-mentioned world average. Quasielastic neutrino-nucleon scattering (1) is a basic signal process in neutrino oscillation studies. It is essential to obtain consistency between experiments utilizing different beam energies, and different nuclear targets.

While a number of effects could be causing this tension, we here investigate perhaps the simplest possibility: that the parameterizations of the axial-vector form factor in common use are overly constrained. Such a possibility seems natural, considering that the dipole ansatz has been found to conflict with electron scattering data for the vector form factors. We do not offer new insight on whether other effects, such as nuclear modeling, could also be biasing measurements. However, we point out that by gaining firm control over the nucleon-level amplitude, such nuclear physics effects can be robustly isolated.

The axial mass parameter as introduced in (2) is not well-defined, since the true form factor of the proton does not have a pure dipole behavior. Sufficiently precise measurements forced to fit this functional form will necessarily find different values for m_A^{dipole} resulting from sensitivity to different ranges of q^2. Let us *define* the axial mass parameter in terms of the form factor slope at $q^2 = 0$: $m_A = [F_A'(0)/2F_A(0)]^{-1/2}$. This definition is model-independent, and allows us to sensibly address tensions between different measurements. To avoid confusion, whenever (2) is used we refer to the extracted parameter as m_A^{dipole}. We will show that the slope at

---

[1]The difference 0.055 is a correction to the conventional representation of the pion electroproduction amplitude, as predicted by heavy baryon chiral perturbation theory [6].

$q^2 = 0$ is essentially the only relevant shape parameter for current data at $Q^2 \lesssim 1\,\mathrm{GeV}^2$, and introduce the formalism to systematically account for the impact of other poorly constrained shape parameters on the determination of m_A. A related study of the vector form factors of the nucleon was presented in [9].

The paper is structured as follows. In Section 2 we discuss the application of analyticity and dispersion relations to the axial-vector form factor of the nucleon. Section 3 presents results for the extraction of the axial-vector form factor slope from MiniBooNE data. We illustrate constraints imposed by our analysis on nuclear models, by determining the binding energy parameter in the Relativistic Fermi Gas (RFG) model of Smith and Moniz [16]. Section 4 gives an illustrative analysis of constraints on the axial mass parameter from pion electroproduction data. Section 5 discusses the implications of our results. For completeness, Appendix A collects formulas for the RFG nuclear model.

2   Analyticity constraints

This section provides form factor definitions and details of the model-independent parameterization based on analyticity.

2.1   Form factor definitions

The nucleon matrix element of the Standard Model weak charged current is

$$\langle p(p')|J_W^{+\mu}|n(p)\rangle \propto \bar{u}^{(p)}(p')\bigg\{\gamma^\mu F_1(q^2) + \frac{i}{2m_N}\sigma^{\mu\nu}q_\nu F_2(q^2)$$

$$+ \gamma^\mu\gamma_5 F_A(q^2) + \frac{1}{m_N}q^\mu\gamma_5 F_P(q^2)\bigg\}u^{(n)}(p)\,, \quad (3)$$

where $q^\mu = p'^\mu - p^\mu$, and we have enforced time-reversal invariance and neglected isospin-violating effects as discussed in Appendix A. The vector form factors $F_1(q^2)$ and $F_2(q^2)$ can be related via isospin symmetry to the electromagnetic form factors measured in electron-nucleon scattering. At low energy, the form factors are normalized as $F_1(0) = 1$, $F_2(0) = \mu_p - \mu_n - 1$. For definiteness we take a common nucleon mass, $m_N \equiv (m_p + m_n)/2$. Parameter values used in the numerical analysis are listed in Table 2. In applications to quasielastic electron- or muon-neutrino scattering, the impact of F_P is suppressed by powers of the small lepton-nucleon mass ratio. For our purposes, the pion pole approximation is sufficient,[2]

$$F_P(q^2) \approx \frac{2m_N^2}{m_\pi^2 - q^2}F_A(q^2)\,. \quad (4)$$

The axial-vector form factor is normalized at $q^2 = 0$ by neutron beta decay (see Table 2). Our main focus is on determining the q^2 dependence of $F_A(q^2)$ in the physical region of

---

[2]Here and throughout, $m_\pi = 140\,\mathrm{MeV}$ denotes the pion mass.

2

quasielastic neutrino scattering, $Q^2 = -q^2 \geq 0$. As discussed in the Introduction, an expansion at $q^2 = 0$ defines an "axial mass parameter" m_A, via

$$F_A(q^2) = F_A(0) \left[1 + \frac{2}{m_A^2} q^2 + \ldots \right] \implies m_A \equiv \sqrt{\frac{2F_A(0)}{F_A'(0)}} \, . \tag{5}$$

Equivalently, we may define an "axial radius" r_A, via

$$F_A(q^2) = F_A(0) \left[1 + \frac{r_A^2}{6} q^2 + \ldots \right] \implies r_A \equiv \sqrt{\frac{6F_A'(0)}{F_A(0)}} \, . \tag{6}$$

The factors appearing in (5) and (6) are purely conventional, motivated by the dipole ansatz (2), and by the analogous charge-radius definition for the vector form factors. Asymptotically, perturbative QCD predicts [10, 11] a $\sim 1/Q^4$ scaling, up to logarithms, for the axial-vector form factor. However, the region $Q^2 \lesssim 1\,\mathrm{GeV}^2$ is far from asymptotic, and the functional dependence of $F_A(q^2)$ remains poorly constrained at accessible neutrino energies.
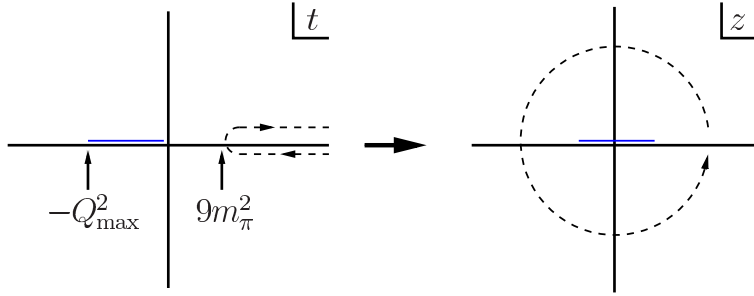
2.2 Analyticity

Figure 1: Conformal mapping of the cut plane to the unit circle.

We proceed along lines similar to the vector form factor analysis in [9]. Recall the dispersion relation for the form factor,

$$F_A(t) = \frac{1}{\pi} \int_{t_{\mathrm{cut}}}^{\infty} dt' \, \frac{\mathrm{Im} F_A(t' + i0)}{t' - t} \, , \tag{7}$$

where $t \equiv q^2$ and the integral starts at the three-pion cut, $t_{\mathrm{cut}} = 9m_\pi^2$. We can make use of this model-independent knowledge by noticing that the separation between the singular region, $t \geq t_{\mathrm{cut}}$, and the kinematically allowed physical region, $t \leq 0$, implies the existence of a small expansion parameter, $|z| < 1$. As illustrated in Fig. 1, by a standard transformation, we map the domain of analyticity onto the unit circle in such a way that the physical region is mapped onto an interval:

$$z(t, t_{\mathrm{cut}}, t_0) = \frac{\sqrt{t_{\mathrm{cut}} - t} - \sqrt{t_{\mathrm{cut}} - t_0}}{\sqrt{t_{\mathrm{cut}} - t} + \sqrt{t_{\mathrm{cut}} - t_0}} \, , \tag{8}$$

3

	$t_0 = 0$	$t_0 = t_0^{\mathrm{opt}}(1.0\,\mathrm{GeV}^2)$
$||F_A||_2/|F_A(t_0)|$	1.5-1.7	1.9-2.3
$||F_A||_\infty/|F_A(t_0)|$	1.0-1.4	1.4-1.8

Table 1: Typical bounds on the coefficient ratios $\sqrt{\sum_k a_k^2/a_0^2}$ (first line of table) and $|a_k/a_0|$ (second line) in an axial-vector dominance ansatz. The range corresponds to the range $250 - 600\,\mathrm{MeV}$ for the a_1 width and the range $1190 - 1270\,\mathrm{MeV}$ for the a_1 mass.

where t_0 is a free parameter representing the point mapping onto $z = 0$. Analyticity implies that the form factor can be expressed as a power series in the new variable,

$$F_A(q^2) = \sum_{k=0}^{\infty} a_k z(q^2)^k \,. \tag{9}$$

The coefficients a_k are bounded in size, guaranteeing convergence of the series. Knowledge of $\mathrm{Im}\, F_A$ over the cut translates into information about the coefficients in the z expansion [9]. In particular we have

$$a_0 = \frac{1}{\pi} \int_0^\pi d\theta \, \mathrm{Re}\, F_A[t(\theta) + i0] = F_A(t_0) \,,$$

$$a_{k\geq 1} = -\frac{2}{\pi} \int_0^\pi d\theta \, \mathrm{Im}\, F_A[t(\theta) + i0] \, \sin(k\theta) = \frac{2}{\pi} \int_{t_{\mathrm{cut}}}^\infty \frac{dt}{t - t_0} \sqrt{\frac{t_{\mathrm{cut}} - t_0}{t - t_{\mathrm{cut}}}} \mathrm{Im} F_A(t) \sin[k\theta(t)] \,, \tag{10}$$

where

$$t = t_0 + \frac{2(t_{\mathrm{cut}} - t_0)}{1 - \cos\theta} \equiv t(\theta) \,. \tag{11}$$

2.3 Coefficient bounds

For a given kinematic range $0 \leq -t \leq Q_{\mathrm{max}}^2$, we can choose the free parameter t_0 in (8) to minimize the resulting maximum size of $|z|$. It is straightforward to see that the "optimal" value of t_0 is $t_0^{\mathrm{opt}} = t_{\mathrm{cut}}\left(1 - \sqrt{1 + Q_{\mathrm{max}}^2/t_{\mathrm{cut}}}\right)$, and for this value of t_0, $|z| \leq [(1 + Q_{\mathrm{max}}^2/t_{\mathrm{cut}})^{1/4} - 1]/[(1 + Q_{\mathrm{max}}^2/t_{\mathrm{cut}})^{1/4} + 1]$. For example, if the kinematic range is $Q_{\mathrm{max}}^2 \lesssim 1\,\mathrm{GeV}^2$, then our expansion parameter is constrained to be $|z| \lesssim 0.2$. Terms beyond linear order in the expansion are suppressed by $|z|^2 \lesssim 0.04$, etc., and are not tightly constrained by current experimental data. This is the sense in which the slope of the form factor (conventionally taken at $q^2 = 0$) is essentially the only relevant shape parameter. The effects of the higher order terms must of course be accounted for in assessing the uncertainty on extracted observables. We now turn to this question.

The expansion coefficients appearing in (9) can be used to define norms,

$$||F_A||_p = \left(\sum_k |a_k|^p\right)^{1/p} \,. \tag{12}$$

4

In particular, $||F_A||_\infty = \sup_k |a_k| = \lim_{p \to \infty} ||F_A||_p$ provides a bound on the maximum coefficient size. The finiteness of the integral appearing in the relation

$$||F_A||_2 = \left(\frac{1}{\pi} \int_{t_{\text{cut}}}^{\infty} \frac{dt}{t - t_0} \sqrt{\frac{t_{\text{cut}} - t_0}{t - t_{\text{cut}}}} |F_A(t)|^2 \right)^{1/2} , \qquad (13)$$

together with $||F_A||_\infty \leq ||F_A||_2$, establishes that a finite upper bound exists for the coefficients. As a first approach to estimating the actual bound $||F_A||_\infty$, consider an "axial-vector dominance" ansatz, $F_A \sim m_{a_1}^2/(m_{a_1}^2 - t - i\Gamma_{a_1} m_{a_1})$, where $m_{a_1} = 1230(40)\,\text{MeV}$ and $\Gamma_{a_1} = 250 - 600\,\text{MeV}$ are the mass and width of the lowest lying axial-vector, iso-vector meson [12]. More precisely, let us define the form factor via its dispersion relation with [13]

$$\text{Im} F_A(t + i0) = \frac{\mathcal{N} m_{a_1}^3 \Gamma_{a_1}}{(t - m_{a_1}^2)^2 + \Gamma_{a_1}^2 m_{a_1}^2} \theta(t - t_{\text{cut}}) , \qquad (14)$$

where $\mathcal{N}$ is a normalization constant determined below. Using the dispersion relation (7) with (14) we find,

$$F_A(t + i0) = \frac{\mathcal{N}}{\pi} \frac{m_{a_1}^3 \Gamma_{a_1}}{|b(t)|^2} \left[\frac{1}{2} \log \left(\frac{|b(t_{\text{cut}})|^2}{|t_{\text{cut}} - t|^2} \right) + \frac{m_{a_1}^2 - t}{m_{a_1} \Gamma_{a_1}} \arg[b(t_{\text{cut}})] + i\pi \theta(t - t_{\text{cut}}) \right] , \qquad (15)$$

where $b(t) = t - m_{a_1}^2 + i\Gamma_{a_1} m_{a_1}$, and $\mathcal{N}$ is determined by the value of $F_A(0)$. Table 1 displays the values for $||F_A||_2$ and $||F_A||_\infty$ computed in this ansatz. For the latter quantity one can show that

$$\left| \frac{a_k}{a_0} \right| \leq \frac{2|\mathcal{N}|}{|F_A(t_0)|} \text{Im} \left(\frac{-m_{a_1}^2}{b(t_{\text{cut}}) + \sqrt{(t_{\text{cut}} - t_0)b(t_{\text{cut}})}} \right) . \qquad (16)$$

While this model is not a rigorous description of the true spectral function in (7), it indicates an order unity bound on the coefficients appearing in (9). Additional support for an order unity bound is provided by a related detailed study of nucleon vector form factors [9], and by form factor studies in a wide range of meson transitions [14, 15].

In the following numerical analysis, we follow [9], and investigate fits with various bounds on coefficients, e.g. $|a_k| \leq 5$ and $|a_k| \leq 10$.

3   Extraction of the axial mass parameter

The MiniBooNE collaboration has presented binned results representing the double differential cross section, $d\sigma/dE_\mu d\cos\theta_\mu$, for the quasielastic scattering process (1) on a neutron bound inside ^{12}C. We apply our description of $F_A(q^2)$ to extract m_A (equivalently, r_A) from the neutrino scattering data, under the assumption of a definite nuclear model, the Relativistic Fermi Gas model [16] as described in Appendix A.

Our theory prediction is obtained using (54), integrating over the energy-dependent ν_μ flux from Table V of [3]; this result is divided by 6 to obtain the per-neutron event rate, and divided by the total flux to obtain the flux-averaged cross section. Corresponding experimental values

Parameter	Value	Reference
$|V_{ud}|$	0.9742	[12]
μ_p	2.793	[12]
μ_n	-1.913	[12]
m_μ	0.1057 GeV	[12]
G_F	1.166×10^{-5} GeV^{-2}	[12]
m_N	0.9389 GeV	[12]
$F_A(0)$	-1.269	[12]
ϵ_b	0.025 GeV	[17]
p_F	0.220 GeV	[3]

Table 2: Numerical values for input parameters.

for the double differential cross section are taken from Table VI of [3]. We form an error matrix,

$$E_{ij} = (\delta\sigma_i)^2 \delta_{ij} + (\delta N)^2 \sigma_i \sigma_j \,, \tag{17}$$

where $\sigma_i = (d\sigma/dE_\mu d\cos\theta_\mu)\Delta E_\mu \Delta \cos\theta_\mu$ denotes a partial cross section, $\delta\sigma_i$ denotes the shape uncertainty from Table VII of [3], and $\delta N = 0.107$ is the normalization error from [3]. We form the chi-squared function

$$\chi^2 = \sum_{ij}(\sigma_i^{\text{expt.}} - \sigma_i^{\text{theory}})E_{ij}^{-1}(\sigma_j^{\text{expt.}} - \sigma_j^{\text{theory}}) \,, \tag{18}$$

and minimize χ^2 to find best fit values for m_A. Error intervals are defined by $\Delta\chi^2 = 1$. The nucleon form factors and the nuclear model employ parameter values listed in Table 2. Following the analysis of [3], the vector form factors F_1 and F_2 are given by the BBA2003 parameterization [18]. We use a default value $\epsilon_b = 0.025$ GeV, as extracted from electron scattering data on nuclei in [17]. This value is different from the central value adopted in the MiniBooNE analysis [3], where $\epsilon_b = 0.034 \pm 0.09$ GeV. We show below that such a high value of ϵ_b is not favored by the MiniBooNE data, but investigate fit results for different values of ϵ_b.

The slope at $q^2 = 0$, and hence m_A from (5) is most sensitive to low-Q^2 data. We analyze this sensitivity by considering the effect of a cut on Q^2. The value of Q^2 for a given value of the observed muon energy and angle can be reconstructed assuming quasielastic scattering on a free neutron, but is not determined unambiguously once nuclear effects are included. As a proxy for Q^2, we define an approximate "reconstructed" Q^2,

$$Q_{\text{rec}}^2 = 2E_\nu^{\text{rec}} E_\mu - 2E_\nu^{\text{rec}}\sqrt{E_\mu^2 - m_\mu^2}\cos\theta_\mu - m_\mu^2 \,, \tag{19}$$

where E_ν^{rec} approximates the neutrino energy in the nucleon rest frame,

$$E_\nu^{\text{rec}} = \frac{m_N E_\mu - m_\mu^2/2}{m_N - E_\mu + \sqrt{E_\mu^2 - m_\mu^2}\cos\theta_\mu} \,. \tag{20}$$

6

We note that Q^2_{rec} coincides with Q^2_{rec} used by K2K in the limit $\epsilon_b \to 0$ [1], and with Q^2_{QE} used by MiniBooNE in the limit $\epsilon_b \to 0$ and equal proton and neutron masses [3]. For simplicity we have chosen to make the cut independent of the binding energy used in the nuclear model. We emphasize that this choice is used simply to define the subset of data to be analyzed, and does introduce theoretical uncertainty in the numerical results.
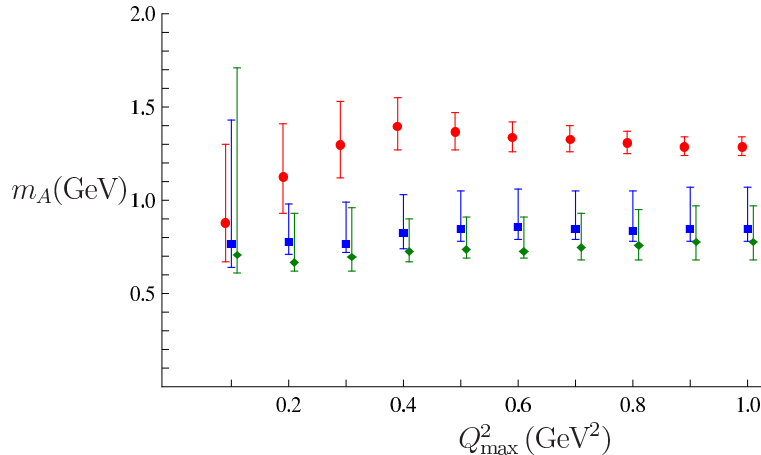

Figure 2: Extracted value of m_A versus Q^2_{max}. Dipole model results for m_A^{dipole} are shown by the red circles; z expansion results with $|a_k| \leq 5$ are shown by the blue squares, z expansion results with $|a_k| \leq 10$ are shown by the green diamonds.

Our results are displayed in Fig. 2, where we compare extractions of m_A^{dipole} in the dipole ansatz (2) with extractions of m_A employing the z expansion (9). We present results for data with $Q^2_{\text{rec}} \leq Q^2_{\text{max}}$, where Q^2_{rec} is defined in (19) and $Q^2_{\text{max}} = 0.1, 0.2, \ldots, 1.0 \, \text{GeV}^2$. We study two different coefficient bounds, $|a_k| \leq 5$ and $|a_k| \leq 10$. For definiteness we have truncated the sum in (9) at $k_{\text{max}} = 7$, but have checked that the results to not change significantly if higher orders are included. As the figure illustrates, the z expansion results lie systematically below results assuming the dipole ansatz. In contrast to results from the one-parameter dipole ansatz, high-Q^2 data have relatively small impact on the model-independent determination of m_A. Taking for definiteness $Q^2_{\text{max}} = 1.0 \, \text{GeV}^2$, we find

$$m_A = 0.85^{+0.22}_{-0.07} \pm 0.09 \, \text{GeV} \qquad \text{(neutrino scattering)}, \qquad (21)$$

where the first error is experimental, using the fit with $|a_k| \leq 5$, and the second error represents residual form factor shape uncertainty, taken as the maximum change of the 1σ interval when the bound is increased to $|a_k| \leq 10$. As a comparison, a fit assuming the dipole form factor, and the same Q^2_{max} yields $m_A^{\text{dipole}} = 1.29 \pm 0.05$ GeV.[3]

It is not our purpose in this paper to investigate in detail the additional uncertainty that should be assigned to (21) due to nuclear effects. We note that a fit of the MiniBooNE data to the RFG model with free parameter ϵ_b yields the value, without an assumption on the value

---

[3]A dipole fit including the entire dataset without a cut on Q^2_{rec} yields $m_A^{\text{dipole}} = 1.28^{+0.03}_{-0.04}$.

of m_A, (for $Q^2_{\max} = 1.0\,\mathrm{GeV}^2$, $k_{\max} = 7$)

$$\epsilon_b = 28 \pm 3\,\mathrm{MeV}\,, \tag{22}$$

where the result is insensitive to the choice of bound, $|a_k| \leq 5$ or $|a_k| \leq 10$.[4] While the data do not appear to favor significantly higher values of ϵ_b, we note that for $\epsilon_b = 34\,\mathrm{MeV}$ [3], the result (21) becomes $m_A(\epsilon_b = 34\,\mathrm{MeV}) = 1.05^{+0.45}_{-0.18} \pm 0.12$, compared to $m_A^{\mathrm{dipole}}(\epsilon_b = 34\,\mathrm{MeV}) = 1.44 \pm 0.05$.

We have performed fits at different values of the parameter t_0, finding no significant deviation in the results. The results do not depend strongly on the precise value of the bound (e.g. $|a_k| \leq 5$ versus $|a_k| \leq 10$). Similar to [9], we conclude that the estimation of shape uncertainty in (21) should be conservative. The fit (21) yields coefficients[5] $a_0 \equiv F_A(0) = -1.269$, $a_1 = 2.9^{+1.1}_{-1.0}$, $a_2 = -8^{+6}_{-3}$. These values are in accordance with our assumption of order-unity coefficient bounds. As discussed in the Introduction, current experiments do not significantly constrain shape parameters beyond the linear term, a_1.
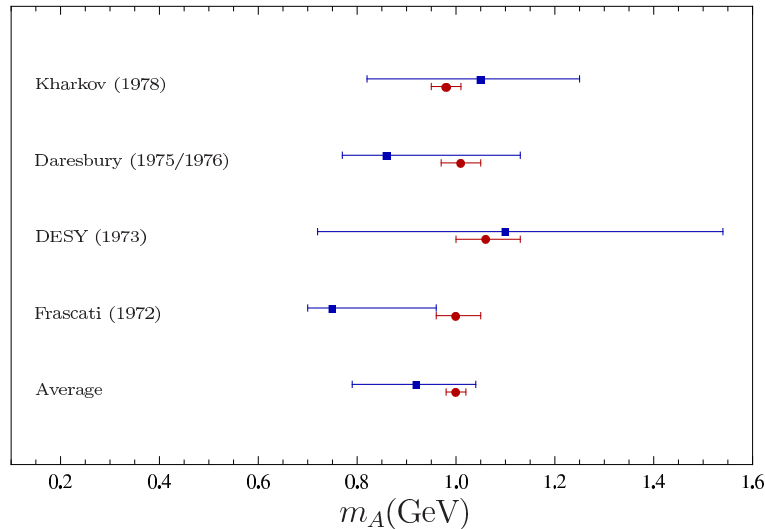
4   Comparison to charged pion electroproduction

Figure 3: Extraction of m_A using charged pion electroproduction measurements, in the dipole ansatz and in the z expansion. Datasets are as described in the text. Dipole results are shown as the red circles, and z expansion results with $|a_k| \leq 5$ are shown as the blue squares.

The axial-vector component of the weak current defining $F_A(q^2)$ in (3) can also be probed in pion electroproduction measurements. The electric dipole amplitude for threshold charged-pion electroproduction obeys a low-energy theorem in the chiral limit relating this amplitude

---

[4]Using a dipole ansatz for $Q^2_{\max} = 1.0\,\mathrm{GeV}^2$ without fixing m_A^{dipole} yields $\epsilon_b = 22 \pm 7\,\mathrm{MeV}$.
[5]For this purpose we take $k_{\max} = 7$ in (9) and enforce $|a_k| \leq 10$ for $k \geq 3$.

to the axial-vector form factor of the nucleon [19]. After applying chiral corrections, such measurements can thus in principle be used to determine m_A. Data for this process have been interpreted in the context of the dipole ansatz (2). We found that the dipole assumption can strongly bias extractions of m_A in neutrino scattering measurements. In order to gauge whether the same statement is true for the electroproduction data, let us apply the z expansion to extract m_A from the inferred $F_A(q^2)$ values for an illustrative dataset, taken from Refs. [20, 21, 22, 23, 24]. We have selected datasets that appear in the compilation [6] (cf. Figure 1 of that reference), and that also explicitly list inferred values of $F_A(q^2)$ (see also [25, 26, 27, 28, 29]). Figure 3 displays extractions of m_A in both the z expansion and the dipole ansatz (2) for each of the five datasets.[6] For the larger bound $|a_k| \leq 10$, the slope of $F_A(q^2)$ is not constrained to be positive by each individual dataset, and we display only the result for $|a_k| \leq 5$. Applying the z expansion to the entire (17 point) dataset, we find

$$m_A = 0.92^{+0.12}_{-0.13} \pm 0.08 \, \text{GeV} \qquad (\text{electroproduction}) \,, \tag{23}$$

where the errors are experimental, and from residual shape uncertainty, as in (21). In contrast, a fit of the same data to the dipole ansatz yields $m_A^{\text{dipole}} = 1.00 \pm 0.02 \, \text{GeV}$. These averages are also displayed in the figure. We emphasize that our chosen dataset is not exhaustive We have not attempted to address questions such as correlations between different datasets, or uncertainties from model-dependent hard-pion corrections. We leave a more detailed treatment to future work.

5   Summary

We have presented a model independent description of the axial-vector form factor of the nucleon. This form factor plays a crucial role in neutrino quasielastic scattering at accelerator energies, which is a basic signal process for neutrino oscillation studies, and is an important ingredient in normalizing the neutrino flux at detector locations. Recent tensions between measurements in neutrino scattering at different energies, and between neutrino scattering and pion electroproduction measurements indicate a problem in our understanding of this elementary process.

Several studies have tried to address these discrepancies. Modified nuclear models [31, 32, 33] have been used to find an axial mass close to the MiniBooNE result. Other nuclear models include effects of multi-nucleon emission [34, 35, 36, 37, 38, 39], and have been reported to obtain better agreement with the differential MiniBooNE data from [3]. One of these studies [39] reports a dipole axial mass extracted from MiniBooNE data in agreement with world averages from [6, 5]. Another group [40], modifies the magnetic form factor G_M for nucleons bound in carbon but does not change the form factors G_E or F_A. The assumption of the dipole ansatz (2) is a crucial element in many of these studies.[7] Our analysis shows that

---

[6]For definiteness, where necessary we have chosen one amongst different models for applied hard-pion corrections: the BNR prescription [30] in [22, 23, 24], and the BNR prescription with first form factor assumption in [20] ("$F_\pi = F_1^V$" in Table 2 of [20]). We have combined the low-Q^2 and high-Q^2 data from [22] and [23] to obtain the Daresbury(1975/1976) data point in Fig. 3.

[7]A parameterization that modifies the dipole behavior at large Q^2 is presented in [41].

this ansatz introduces a strong bias in measurements, which must be addressed in order to disentangle nucleon-level interactions from nuclear effects.

Under the assumption of a definite nuclear model (the RFG model, summarized in Appendix A, with parameter values as in Table 2), we extract m_A as defined model-independently in (5) from the differential MiniBooNE data [3]. The result is displayed in (21), $m_A = 0.85^{+0.22}_{-0.07} \pm 0.09 \, \mathrm{GeV}$. This result may be contrasted with a fit to an illustrative dataset for pion electroproduction displayed in (23), $m_A = 0.92^{+0.12}_{-0.13} \pm 0.08 \, \mathrm{GeV}$. These values may be compared to fits using the dipole ansatz (2): $m_A^{\mathrm{dipole}} = 1.29 \pm 0.05 \, \mathrm{GeV}$ (neutrino scattering) and $m_A^{\mathrm{dipole}} = 1.00 \pm 0.02 \, \mathrm{GeV}$ (electroproduction). A discrepancy is apparent in the dipole ansatz (2), but can be ascribed to the unjustified and restrictive assumption on the form factor shape. After gaining firm control over the nucleon-level amplitude, nuclear effects can be robustly isolated. For example, in the context of the RFG model, we extract the result (22) for the binding energy parameter ϵ_b.

The axial mass parameter, or equivalently, the axial radius (6), is a fundamental parameter of nucleon structure. The results (21),(23) can be expressed as

$$
r_A = \begin{cases} 0.80^{+0.07}_{-0.17} \pm 0.12 \, \mathrm{fm} & \text{(neutrino scattering)} \\ 0.74^{+0.12}_{-0.09} \pm 0.05 \, \mathrm{fm} & \text{(electroproduction)} \end{cases} . \tag{24}
$$

More precise measurements in both neutrino scattering and pion electroproduction are necessary to substantially reduce the errors on m_A, or equivalently r_A. This would be necessary to provide a model-independent confirmation of the convergence of chiral perturbation theory corrections based on comparison of electroproduction and neutrino scattering data.

A related study of the nucleon vector form factors was presented in [9]. As described there, different expansion "schemes" are possible. For example, we may replace (9) with $\phi(t)F_A(t) = \sum_k a_k z(t)^k$ where ϕ is analytic below t_{cut}. A choice such as $\phi \sim (1 - t/m'^2)^n$ with $m' \sim \mathrm{GeV}$ could be used to enforce a $1/Q^{2n}$ falloff for asymptotic Q^2, while retaining the known analytic structure of the form factor. Such modifications do not significantly impact the extraction of m_A, and we have focused on the simplest choice ($t_0 = 0$ and $\phi = 1$).

Our study indicates that the error on the axial mass parameter extracted using the dipole ansatz is underestimated. While the errors from a model-independent analysis may be larger, it is essential to study model-independent numbers in order to draw firm conclusions. The simulation of more complicated neutrino scattering processes (e.g. pion and photon production), is indirectly affected by enforcing agreement with the quasielastic data. It is important for current and future neutrino experiments [42, 43, 44, 45, 5, 46, 3, 47, 48, 49] to converge on consistent values for fundamental neutrino cross sections.

The analysis presented here can be applied to other neutrino scattering datasets, involving different nuclear targets, and including neutral current scattering and antineutrino scattering. It is interesting to extend the analysis of electroproduction data; more precise low-energy electroproduction measurements have potential to impact the interpretation of future neutrino measurements. It is also of interest to incorporate model-independent constraints into more sophisticated nuclear models.

A Appendix: RFG model for quasielastic neutrino scattering

A number of notations and conventions for the form factors and RFG nuclear model [16] exist in the literature. For completeness we collect here the relevant formulas used in our analysis.

A.1 Nucleon matrix element of the weak current

The relevant part of the weak-interaction Lagrangian is

$$\mathcal{L} = \frac{G_F}{\sqrt{2}} V_{ud}\, \bar{\ell}\gamma^\alpha(1 - \gamma_5)\nu\, \bar{u}\gamma_\alpha(1 - \gamma_5)d + \text{H.c.}. \tag{25}$$

The cross section for $\nu(k) + n(p) \to \ell^-(k') + p(p')$ on a free neutron is

$$\sigma_{\text{free}} = \frac{1}{4|k \cdot p|} \int \frac{d^3k'}{(2\pi)^3 2E_{\boldsymbol{k'}}} \int \frac{d^3p'}{(2\pi)^3 2E_{\boldsymbol{p'}}} \overline{|\mathcal{M}^2|}(2\pi)^4\delta^4(k + p - k' - p'), \tag{26}$$

where the spin-averaged, squared amplitude is

$$\overline{|\mathcal{M}^2|} = \frac{G_F^2|V_{ud}|^2}{4} L^{\mu\nu} \sum_{\text{spins}} \langle p(p')|\bar{u}\gamma_\mu(1 - \gamma_5)d|n(p)\rangle \langle p(p')|\bar{u}\gamma_\nu(1 - \gamma_5)d|n(p)\rangle^*. \tag{27}$$

The leptonic tensor neglecting the neutrino mass is ($\epsilon^{0123} = -1$)

$$L^{\mu\nu} = 8(k^\mu k'^\nu + k^\nu k'^\mu - g^{\mu\nu}k \cdot k' - i\epsilon^{\mu\nu\rho\sigma}k_\rho k'_\sigma). \tag{28}$$

The hadronic matrix element appearing in (27) is parameterized by

$$\langle p(p')|\bar{u}\gamma_\mu(1 - \gamma_5)d|n(p)\rangle = \bar{u}^{(p)}(p')\Gamma_\mu(q)u^{(n)}(p), \tag{29}$$

where $q = k - k' = p' - p$ and we have defined the vertex function

$$\Gamma_\mu(q) = \gamma_\mu F_1(q^2) + \frac{i}{2m_N}\sigma_{\mu\nu}q^\nu F_2(q^2) + \frac{q_\mu}{m_N}F_S(q^2) + \gamma_\mu\gamma_5 F_A(q^2) + \frac{p_\mu + p'_\mu}{m_N}\gamma_5 F_T(q^2)$$

$$+ \frac{q_\mu}{m_N}\gamma_5 F_P(q^2). \tag{30}$$

11

We may write the cross section of (26) as

$$\sigma_{\text{free}} = \frac{G_F^2 |V_{ud}|^2}{16|k \cdot p|} \int \frac{d^3 k'}{(2\pi)^3 2E_{\mathbf{k}'}} L^{\mu\nu} \hat{W}_{\mu\nu} \, , \tag{31}$$

where the nucleon structure function is

$$\hat{W}_{\mu\nu} = \int \frac{d^3 p'}{(2\pi)^3 2E_{\mathbf{p}'}} (2\pi)^4 \delta^4(p - p' + q) H_{\mu\nu} \, . \tag{32}$$

The hadronic tensor is

$$H_{\mu\nu} = \text{Tr}[(\not{p}' + m_p)\Gamma_\mu(q)(\not{p} + m_n)\bar{\Gamma}_\nu(q)] \, , \tag{33}$$

where as usual, $\bar{\Gamma} = \gamma^0 \Gamma^\dagger \gamma^0$. We may similarly analyze antineutrino scattering, $\bar{\nu}(k) + p(p) \to \ell^+(k') + n(p')$, using (31), taking $L^{\mu\nu} \to L^{\nu\mu}$, and making the replacements $m_n \leftrightarrow m_p$, $\Gamma_\mu(q) \to \bar{\Gamma}_\mu(-q)$ in $H_{\mu\nu}$.

Imposing time-reversal invariance shows that $F_i(q^2)$ are real. We will assume isospin symmetry in the following, in which case F_S and F_T vanish, $m_n = m_p = m_N$, and $\bar{\Gamma}_\mu(-q) = \Gamma_\mu(q)$. The hadronic tensor has the time-reversal invariant decomposition

$$H_{\mu\nu} = -g_{\mu\nu} H_1 + \frac{p_\mu p_\nu}{m_N^2} H_2 - i \frac{\epsilon_{\mu\nu\rho\sigma}}{2m_N^2} p^\rho q^\sigma H_3 + \frac{q_\mu q_\nu}{m_N^2} H_4 + \frac{(p_\mu q_\nu + q_\mu p_\nu)}{2m_N^2} H_5 \, . \tag{34}$$

The H_i's are expressed in terms of the form factors F_i as

$$H_1 = 8m_N^2 F_A^2 - 2q^2 \left[(F_1 + F_2)^2 + F_A^2\right] \, ,$$
$$H_2 = H_5 = 8m_N^2 \left(F_1^2 + F_A^2\right) - 2q^2 F_2^2 \, ,$$
$$H_3 = -16m_N^2 F_A(F_1 + F_2) \, ,$$
$$H_4 = -\frac{q^2}{2} \left(F_2^2 + 4F_P^2\right) - 2m_N^2 F_2^2 - 4m_N^2 \left(F_1 F_2 + 2F_A F_P\right) \, . \tag{35}$$

Expressions for complex F_i and nonzero F_S, F_T can be found, for example, in [50].

A.2 Model for the nuclear matrix element

We employ a standard treatment of nuclear effects, the "Relativistic Fermi Gas" (RFG) model as presented by Smith and Moniz in [16], based on the model presented in [51].

We assume that there are A nucleons inside the nucleus, with $A/2$ neutrons and $A/2$ protons. The incoming neutrino interacts with a neutron with 3-momentum $\mathbf{p}$, determined by some distribution $n_i(\mathbf{p})$. The final state proton phase space is limited by a factor of $[1 - n_f(\mathbf{p}')]$ enforcing Fermi statistics. Symbolically,

$$\sigma_{\text{nuclear}} = n_i(\mathbf{p}) \otimes \sigma_{\text{free}}(\mathbf{p} \to \mathbf{p}') \otimes [1 - n_f(\mathbf{p}')], \tag{36}$$

and more explicitly

$$\sigma_{\text{nuclear}} \approx 2V \int \frac{d^3 p}{(2\pi)^3} n_i(\boldsymbol{p})$$

$$\left\{ \frac{G_F^2}{16|k \cdot p|} \int \frac{d^3 k'}{(2\pi)^3 2E_{\boldsymbol{k}'}} \int \frac{d^3 p'}{(2\pi)^3 2E_{\boldsymbol{p}'}} (2\pi)^4 \delta^4(p - p' + q) L^{\mu\nu} H_{\mu\nu} \right\} [1 - n_f(\boldsymbol{p}')] . \quad (37)$$

To arrive at the final model, two modifications are made. First, we make the replacement $k \cdot p \to E_{\boldsymbol{k}} E_{\boldsymbol{p}}$ in the prefactor of (37). This replacement ignores a correction from the nonzero velocity of the initial state nucleon. It corresponds to the model of [16], adopted by [3]; for definiteness we have followed this convention. Second, we incorporate a "binding energy", ϵ_b, by expressing $H_{\mu\nu}$ as a function of Lorentz 4-vectors p_μ, q_μ as in (34) and then making in (37) the replacements

$$p^0 \to \epsilon_{\boldsymbol{p}} \equiv E_{\boldsymbol{p}} - \epsilon_b , \quad p'^0 \to \epsilon'_{\boldsymbol{p}'} \equiv E_{\boldsymbol{p}'} , \quad (38)$$

with $E_{\boldsymbol{p}} \equiv \sqrt{m_N^2 + |\boldsymbol{p}|^2}$. Again, there is some arbitrariness to the insertion of ϵ_b into the formalism; for definiteness we have followed the conventions of [16]. The cross section is then

$$\sigma_{\text{nuclear}} = \frac{G_F^2}{16|k \cdot p_T|} \int \frac{d^3 k'}{(2\pi)^3 2E_{\boldsymbol{k}'}} L^{\mu\nu} W_{\mu\nu} , \quad (39)$$

where p_T^μ is the 4-momentum of the target nucleus with mass $m_T \equiv A m_N (1 - \epsilon_b)$. We work in the target rest frame where $p_T^\mu = m_T \delta_0^\mu$. The model nuclear structure function $W_{\mu\nu}$ is defined as

$$W_{\mu\nu} \equiv \int d^3 p \, f(\boldsymbol{p}, q^0, \boldsymbol{q}) H_{\mu\nu}(\epsilon_{\boldsymbol{p}}, \boldsymbol{p}; q^0, \boldsymbol{q}) , \quad (40)$$

with

$$f(\boldsymbol{p}, q^0, \boldsymbol{q}) = \frac{m_T V}{4\pi^2} n_i(\boldsymbol{p})[1 - n_f(\boldsymbol{p} + \boldsymbol{q})] \frac{\delta(\epsilon_{\boldsymbol{p}} - \epsilon'_{\boldsymbol{p}+\boldsymbol{q}} + q^0)}{\epsilon_{\boldsymbol{p}} \epsilon'_{\boldsymbol{p}+\boldsymbol{q}}} . \quad (41)$$

The distribution of neutrons and protons is

$$n_i(\boldsymbol{p}) = \theta(p_F - |\boldsymbol{p}|) , \quad n_f(\boldsymbol{p}') = \theta(p_F - |\boldsymbol{p}'|) , \quad (42)$$

where p_F is a parameter of the model. The normalization V is fixed by requiring $A/2$ neutrons below the Fermi surface (accounting for 2 fermionic spin states),

$$\frac{A}{2} = 2V \int \frac{d^3 p}{(2\pi)^3} n_i(\boldsymbol{p}) \implies V = \frac{3\pi^2 A}{2p_F^3} . \quad (43)$$

We can expand $W_{\mu\nu}$ in a similar way to $H_{\mu\nu}$ in (34):

$$W_{\mu\nu} = -g_{\mu\nu} W_1 + \frac{p_\mu^T p_\nu^T}{m_T^2} W_2 - i \frac{\epsilon_{\mu\nu\rho\sigma}}{2m_T^2} p_T^\rho q^\sigma W_3 + \frac{q_\mu q_\nu}{m_T^2} W_4 + \frac{(p_\mu^T q_\nu + q_\mu p_\nu^T)}{2m_T^2} W_5 . \quad (44)$$

13

The functions W_i are related to integrals over H_i. The relations can be expressed in terms of the following integrals [16]:

$$a_1 = \int d^3p\, f(\boldsymbol{p}, q)\,, \qquad\qquad a_2 = \int d^3p\, f(\boldsymbol{p}, q)\, \frac{|\boldsymbol{p}|^2}{m_N^2}\,,$$

$$a_3 = \int d^3p\, f(\boldsymbol{p}, q)\, \frac{(p^z)^2}{m_N^2}\,, \qquad\qquad a_4 = \int d^3p\, f(\boldsymbol{p}, q)\, \frac{\epsilon_{\boldsymbol{p}}^2}{m_N^2}\,,$$

$$a_5 = \int d^3p\, f(\boldsymbol{p}, q)\, \frac{\epsilon_{\boldsymbol{p}} p^z}{m_N^2}\,, \qquad\qquad a_6 = \int d^3p\, f(\boldsymbol{p}, q)\, \frac{p^z}{m_N}\,,$$

$$a_7 = \int d^3p\, f(\boldsymbol{p}, q)\, \frac{\epsilon_{\boldsymbol{p}}}{m_N}\,, \tag{45}$$

where $|\boldsymbol{p}|^2 = (p^x)^2 + (p^y)^2 + (p^z)^2$ and the z axis is parallel to $\boldsymbol{q}$. A straightforward but tedious comparison shows that

$$W_1 = a_1 H_1 + \frac{1}{2}(a_2 - a_3) H_2\,,$$

$$W_2 = \left[a_4 + \frac{\omega^2}{|\boldsymbol{q}|^2} a_3 - 2\frac{\omega}{|\boldsymbol{q}|} a_5 + \frac{1}{2}\left(1 - \frac{\omega^2}{|\boldsymbol{q}|^2}\right)(a_2 - a_3)\right] H_2\,,$$

$$W_3 = \frac{m_T}{m_N}\left(a_7 - \frac{\omega}{|\boldsymbol{q}|} a_6\right) H_3\,,$$

$$W_4 = \frac{m_T^2}{m_N^2}\left[a_1 H_4 + \frac{m_N}{|\boldsymbol{q}|} a_6 H_5 + \frac{m_N^2}{2|\boldsymbol{q}|^2}(3a_3 - a_2) H_2\right]\,,$$

$$W_5 = \frac{m_T}{m_N}\left(a_7 - \frac{\omega}{|\boldsymbol{q}|} a_6\right) H_5 + \frac{m_T}{|\boldsymbol{q}|}\left[2a_5 + \frac{\omega}{|\boldsymbol{q}|}(a_2 - 3a_3)\right] H_2\,, \tag{46}$$

where we are using $\omega = q^0$. Recall that the H_i are functions of $q^2 = \omega^2 - |\boldsymbol{q}|^2$. For the integrals a_i let us define $\omega_{\text{eff}} = \omega - \epsilon_b$, and observe that

$$\delta(\epsilon_{\boldsymbol{p}} - \epsilon_{\boldsymbol{p}+\boldsymbol{q}} + q^0) = \delta(E_{\boldsymbol{p}} - E_{\boldsymbol{p}+\boldsymbol{q}} + \omega_{\text{eff}}) = \frac{E_{\boldsymbol{p}+\boldsymbol{q}}}{|\boldsymbol{p}||\boldsymbol{q}|}\delta\left(\cos\theta_{pq} - \frac{\omega_{\text{eff}}^2 - |\boldsymbol{q}|^2 + 2\omega_{\text{eff}} E_{\boldsymbol{p}}}{2|\boldsymbol{p}||\boldsymbol{q}|}\right)\,. \tag{47}$$

The integrals a_i can be expressed in terms of

$$b_j = \frac{m_T V}{2\pi|\boldsymbol{q}|}\int dE_{\boldsymbol{p}}\frac{E_{\boldsymbol{p}}}{E_{\boldsymbol{p}} - \epsilon_b}\left(\frac{E_{\boldsymbol{p}}}{m_N}\right)^j\,, \tag{48}$$

for $j = 0, 1, 2$. In particular,

$$b_0 = \frac{m_T V}{2\pi|\boldsymbol{q}|}\left(E + \epsilon_b \log(E - \epsilon_b)\right)\Big|_{E_{\text{lo}}}^{E_{\text{hi}}}\,,$$

14

$$b_1 = \frac{m_T V}{2\pi m_N |\boldsymbol{q}|} \left[\frac{1}{2}E^2 + \epsilon_b \left(E + \epsilon_b \log(E - \epsilon_b) \right) \right] \Bigg|_{E_{\mathrm{lo}}}^{E_{\mathrm{hi}}},$$

$$b_2 = \frac{m_T V}{2\pi m_N^2 |\boldsymbol{q}|} \left\{ \frac{1}{3}E^3 + \epsilon_b \left[\frac{1}{2}E^2 + \epsilon_b \left(E + \epsilon_b \log(E - \epsilon_b) \right) \right] \right\} \Bigg|_{E_{\mathrm{lo}}}^{E_{\mathrm{hi}}}. \quad (49)$$

Up to an overall constant these are the b_i's of [16]. Introducing $c = -\omega_{\mathrm{eff}}/|\boldsymbol{q}|$, $d = -(\omega_{\mathrm{eff}}^2 - |\boldsymbol{q}|^2)/(2|\boldsymbol{q}|m_N)$, we can express the a_i's as

$$a_1 = b_0 , \quad a_2 = b_2 - b_0 , \quad a_3 = c^2 b_2 + 2cd b_1 + d^2 b_0 , \quad a_4 = b_2 - \frac{2\epsilon_b}{m_N} b_1 + \frac{\epsilon_b^2}{m_N^2} b_0 ,$$

$$a_5 = -cb_2 + \left(\frac{\epsilon_b}{m_N}c - d \right) b_1 + \frac{\epsilon_b}{m_N} d b_0 , \quad a_6 = -cb_1 - db_0 , \quad a_7 = b_1 - \frac{\epsilon_b}{m_N} b_0 . \quad (50)$$

The range of integration is restricted by the conditions,

$$E_{\boldsymbol{p}} \le E_F \equiv \sqrt{m_N^2 + p_F^2} \le E_{\boldsymbol{p}+\boldsymbol{q}} = E_{\boldsymbol{p}} + \omega_{\mathrm{eff}} , \quad -1 \le \frac{\omega_{\mathrm{eff}}^2 - |\boldsymbol{q}|^2 + 2\omega_{\mathrm{eff}} E_{\boldsymbol{p}}}{2|\boldsymbol{q}|\sqrt{E_{\boldsymbol{p}}^2 - m_N^2}} \le 1 . \quad (51)$$

The latter condition can be expressed as

$$\left(\frac{E_{\boldsymbol{p}}}{m_N} - \frac{cd + \sqrt{1 - c^2 + d^2}}{1 - c^2} \right) \left(\frac{E_{\boldsymbol{p}}}{m_N} - \frac{cd - \sqrt{1 - c^2 + d^2}}{1 - c^2} \right) \ge 0 . \quad (52)$$

Define

$$E_{\mathrm{lo}} = \max \left(E_F - \omega_{\mathrm{eff}}, \; m_N \frac{cd + \sqrt{1 - c^2 + d^2}}{1 - c^2} \right) , \quad E_{\mathrm{hi}} = E_F . \quad (53)$$

Then if $E_{\mathrm{lo}} \ge E_{\mathrm{hi}}$, there is no contribution for the given kinematics.

In the rest frame of the nucleus, let E_ℓ and $|\vec{P}_\ell| = \sqrt{E_\ell^2 - m_\ell^2}$ be the energy and 3-momentum of the charged lepton, and let θ_ℓ be the angle between the 3-momenta of the leptons. From (39), the final expression for the differential cross section of neutrino-nucleus scattering is

$$\frac{d\sigma_{\mathrm{nuclear}}}{dE_\ell d\cos\theta_\ell} = \frac{G_F^2 |\vec{P}_\ell|}{16\pi^2 m_T} \left\{ 2(E_\ell - |\vec{P}_\ell| \cos\theta_\ell) W_1 + (E_\ell + |\vec{P}_\ell| \cos\theta_\ell) W_2 \right.$$

$$\left. \pm \frac{1}{m_T} \left[(E_\ell - |\vec{P}_\ell| \cos\theta_\ell)(E_\nu + E_\ell) - m_\ell^2 \right] W_3 + \frac{m_\ell^2}{m_T^2}(E_\ell - |\vec{P}_\ell| \cos\theta_\ell) W_4 - \frac{m_\ell^2}{m_T} W_5 \right\}, \quad (54)$$

where W_i are given in (46), and where the upper (lower) sign is for neutrino (anti-neutrino) scattering.

15

References

[1] R. Gran *et al.* [K2K Collaboration], Phys. Rev. D **74**, 052002 (2006) [arXiv:hep-ex/0603034].

[2] A. A. Aguilar-Arevalo *et al.* [MiniBooNE Collaboration], Phys. Rev. Lett. **100**, 032301 (2008) [arXiv:0706.0926 [hep-ex]].

[3] A. A. Aguilar-Arevalo *et al.* [MiniBooNE Collaboration], arXiv:1002.2680 [hep-ex].

[4] A. A. Aguilar-Arevalo *et al.* [MiniBooNE Collaboration], Phys. Rev. D **82**, 092005 (2010) [arXiv:1007.4730 [hep-ex]].

[5] V. Lyubushkin *et al.* [NOMAD Collaboration], Eur. Phys. J. C **63**, 355 (2009) [arXiv:0812.4543 [hep-ex]].

[6] V. Bernard, L. Elouadrhiri and U. G. Meissner, J. Phys. G **28**, R1 (2002) [arXiv:hep-ph/0107088].

[7] X. Espinal and F. Sanchez, AIP Conf. Proc. **967**, 117 (2007).

[8] M. Dorman [MINOS Collaboration], AIP Conf. Proc. **1189**, 133 (2009).

[9] R. J. Hill and G. Paz, Phys. Rev. D **82**, 113005 (2010) [arXiv:1008.4619 [hep-ph]].

[10] G. P. Lepage and S. J. Brodsky, Phys. Rev. D **22**, 2157 (1980).

[11] C. E. Carlson and J. L. Poor, Phys. Rev. D **34**, 1478 (1986).

[12] K. Nakamura *et al.* [Particle Data Group], J. Phys. G **37**, 075021 (2010).

[13] J. Schwinger, Annals Phys. **9**, 169-193 (1959).

[14] For a review and further references see: R. J. Hill, [arXiv:hep-ph/0606023].

[15] C. Bourrely, B. Machet and E. de Rafael, Nucl. Phys. B **189**, 157 (1981). C. G. Boyd, B. Grinstein and R. F. Lebed, Phys. Rev. Lett. **74**, 4603 (1995) [arXiv:hep-ph/9412324]. L. Lellouch, Nucl. Phys. B **479**, 353 (1996) [arXiv:hep-ph/9509358]. M. C. Arnesen, B. Grinstein, I. Z. Rothstein and I. W. Stewart, Phys. Rev. Lett. **95**, 071802 (2005) [arXiv:hep-ph/0504209]. C. G. Boyd, B. Grinstein and R. F. Lebed, Nucl. Phys. B **461**, 493 (1996) [arXiv:hep-ph/9508211]. I. Caprini, L. Lellouch and M. Neubert, Nucl. Phys. B **530**, 153 (1998) [arXiv:hep-ph/9712417]. T. Becher and R. J. Hill, Phys. Lett. B **633**, 61 (2006) [arXiv:hep-ph/0509090]. R. J. Hill, Phys. Rev. D **74**, 096006 (2006) [arXiv:hep-ph/0607108]. A. Bharucha, T. Feldmann and M. Wick, arXiv:1004.3249 [hep-ph]. C. Bourrely, I. Caprini and L. Lellouch, Phys. Rev. D **79**, 013008 (2009) [arXiv:0807.2722 [hep-ph]].

[16] R. A. Smith and E. J. Moniz, Nucl. Phys. B **43**, 605 (1972) [Erratum-ibid. B **101**, 547 (1975)].

[17] E. J. Moniz, I. Sick, R. R. Whitney, J. R. Ficenec, R. D. Kephart and W. P. Trower, Phys. Rev. Lett. **26**, 445 (1971).

[18] H. S. Budd, A. Bodek and J. Arrington, arXiv:hep-ex/0308005.

[19] Y. Nambu and D. Lurie, Phys. Rev. **125**, 1429 (1962). Y. Nambu and E. Shrauner, Phys. Rev. **128**, 862 (1962).

[20] E. Amaldi *et al.*, Phys. Lett. B **41**, 216 (1972).

[21] P. Brauel *et al.*, Phys. Lett. B **45**, 389 (1973).

[22] A. Del Guerra *et al.*, Nucl. Phys. B **99**, 253 (1975).

[23] A. Del Guerra *et al.*, Nucl. Phys. B **107**, 65 (1976).

[24] A. S. Esaulov, A. M. Pilipenko and Yu. I. Titov, Nucl. Phys. B **136**, 511 (1978).

[25] E. Amaldi *et al.*, Nuovo Cim. A **65**, 377 (1970).

[26] E. D. Bloom *et al.*, Phys. Rev. Lett. **30**, 1186 (1973).

[27] P. Joos *et al.*, Phys. Lett. B **62**, 230 (1976).

[28] S. Choi *et al.*, Phys. Rev. Lett. **71**, 3927 (1993).

[29] A. Liesenfeld *et al.* [A1 Collaboration], Phys. Lett. B **468**, 20 (1999) [arXiv:nucl-ex/9911003].

[30] G. Benfatto, F. Nicolo and G. C. Rossi, Nucl. Phys. B **50**, 205 (1972). G. Benfatto, F. Nicolo and G. C. Rossi, Nuovo Cim. A **14**, 425 (1973).

[31] A. V. Butkevich, Phys. Rev. **C82**, 055501 (2010). [arXiv:1006.1595 [nucl-th]].

[32] O. Benhar, P. Coletti, D. Meloni, Phys. Rev. Lett. **105**, 132301 (2010). [arXiv:1006.4783 [nucl-th]].

[33] C. Juszczak, J. T. Sobczyk, J. Zmuda, Phys. Rev. **C82**, 045502 (2010). [arXiv:1007.2195 [nucl-th]].

[34] M. Martini, M. Ericson, G. Chanfray, J. Marteau, Phys. Rev. **C80**, 065501 (2009). [arXiv:0910.2622 [nucl-th]].

[35] M. Martini, M. Ericson, G. Chanfray, J. Marteau, Phys. Rev. **C81**, 045502 (2010). [arXiv:1002.4538 [hep-ph]].

[36] J. E. Amaro, M. B. Barbaro, J. A. Caballero, T. W. Donnelly, C. F. Williamson, Phys. Lett. **B696**, 151-155 (2011). [arXiv:1010.1708 [nucl-th]].

[37] J. E. Amaro, M. B. Barbaro, J. A. Caballero, T. W. Donnelly, J. M. Udias, [arXiv:1104.5446 [nucl-th]].

17

[38] J. Nieves, I. Ruiz Simo, M. J. Vicente Vacas, Phys. Rev. **C83**, 045501 (2011). [arXiv:1102.2777 [hep-ph]]

[39] J. Nieves, I. R. Simo, M. J. V. Vacas, [arXiv:1106.5374 [hep-ph]].

[40] A. Bodek, H. Budd, [arXiv:1106.0340 [hep-ph]].

[41] A. Bodek, S. Avvakumov, R. Bradford and H. S. Budd, Eur. Phys. J. C **53**, 349 (2008) [arXiv:0708.1946 [hep-ex]].

[42] D. Drakoulakos *et al.* [Minerva Collaboration], arXiv:hep-ex/0405002. D. A. Harris *et al.* [MINERvA Collaboration], arXiv:hep-ex/0410005.

[43] D. S. Ayres *et al.* [NOvA Collaboration], arXiv:hep-ex/0503053.

[44] A. A. Aguilar-Arevalo *et al.* [SciBooNE Collaboration], arXiv:hep-ex/0601022.

[45] H. Chen *et al.* [MicroBooNE Collaboration],

[46] M. C. Sanchez [LBNE DUSEL Collaboration], AIP Conf. Proc. **1222**, 479 (2010). V. Barger *et al.*, arXiv:0705.4396 [hep-ph].

[47] S. D. Holmes [Project X Collaboration], *In the Proceedings of 1st International Particle Accelerator Conference: IPAC'10, Kyoto, Japan, 23-28 May 2010, pp TUYRA01.*

[48] K. Abe *et al.* [T2K Collaboration], arXiv:1106.1238 [Unknown]. K. Abe *et al.* [T2K Collaboration], arXiv:1106.2822 [hep-ex].

[49] S. Choubey *et al.*, "International Design Study for the Neutrino Factory, Interim Design Report," IDS-NF-20, March 2011.

[50] K. S. Kuzmin, V. V. Lyubushkin and V. A. Naumov, Eur. Phys. J. C **54**, 517 (2008) [arXiv:0712.4384 [hep-ph]].

[51] E. J. Moniz, Phys. Rev. **184**, 1154 (1969).